HAL open science

Investigation of cellular instabilities and local extinction for two-phase flames under microgravity conditions

Deniz Kaya Eyice, Fabien Halter, Ahmet Yozgatlıgil, İskender Gökalp, Christian Chauveau

▶ **To cite this version:**

Deniz Kaya Eyice, Fabien Halter, Ahmet Yozgatlıgil, İskender Gökalp, Christian Chauveau. Investigation of cellular instabilities and local extinction for two-phase flames under microgravity conditions. Comptes Rendus. Mécanique, 2023, 351 (S2), pp.1-16. 10.5802/crmeca.174 . hal-04061642

HAL Id: hal-04061642

https://cnrs.hal.science/hal-04061642v1

Submitted on 7 Apr 2023

HAL is a multi-disciplinary open access archive for the deposit and dissemination of scientific research documents, whether they are published or not. The documents may come from teaching and research institutions in France or abroad, or from public or private research centers.

L'archive ouverte pluridisciplinaire **HAL**, est destinée au dépôt et à la diffusion de documents scientifiques de niveau recherche, publiés ou non, émanant des établissements d'enseignement et de recherche français ou étrangers, des laboratoires publics ou privés.

Distributed under a Creative Commons Attribution 4.0 International License

INSTITUT DE FRANCE
Académie des sciences

Comptes Rendus
Mécanique

Deniz Kaya Eyice, Fabien Halter, Ahmet Yozgatlıgil, İskender Gökalp and Christian Chauveau

Investigation of cellular instabilities and local extinction for two-phase flames under microgravity conditions

Published online: 6 April 2023

https://doi.org/10.5802/crmeca.174

Part of Special Issue: Physical Science in Microgravity within the Thematic Group Fundamental and Applied Microgravity

This article is licensed under the
Creative Commons Attribution 4.0 International License.
http://creativecommons.org/licenses/by/4.0/

Les Comptes Rendus. Mécanique *sont membres du Centre Mersenne pour l'édition scientifique ouverte*
www.centre-mersenne.org
e-ISSN : 1873-7234

Comptes Rendus
Mécanique
Published online: 6 April 2023
https://doi.org/10.5802/crmeca.174

Physical Science in Microgravity within the Thematic Group Fundamental and Applied Microgravity / *Sciences physiques en microgravité au sein du GDR Micropesanteur Fondamentale et Appliquée*

Investigation of cellular instabilities and local extinction for two-phase flames under microgravity conditions

Deniz Kaya Eyice *, [a, b, c], **Fabien Halter** [a, b], **Ahmet Yozgatlıgil** [c], **İskender Gökalp** [a, c] **and Christian Chauveau** [a]

[a] CNRS-INSIS, Institut de Combustion, Aérothermique, Réactivité et Environnement, Orléans, 45071, France

[b] Université d'Orléans, Orléans, 45100, France

[c] Department of Mechanical Engineering, Middle East Technical University, Ankara, 06800, Turkey

E-mails: deniz.kaya@cnrs-orleans.fr (D. Kaya Eyice), fabien.halter@cnrs-orleans.fr (F. Halter), ahmety@metu.edu.tr (A. Yozgatlıgil), iskender.gokalp@cnrs-orleans.fr (İ. Gökalp), christian.chauveau@cnrs-orleans.fr (C. Chauveau)

Abstract. The initial mechanism of cellular instabilities on the flame surface was investigated experimentally. Firstly, mono-dispersed ethanol droplets were created via the Wilson cloud principle in a spherical combustion chamber, and aerosol ethanol/air flame propagation was tracked under microgravity conditions. Schlieren images revealed that at the beginning of the cellular structure formation, dark spots formed linking to the signal loss in a density gradient. This phenomenon is assumed to be local extinction and quenching on the flame front due to either liquid droplets' presence or evaporation. To further investigate the observed phenomenon, stagnation flame experiments were performed for rich propane/air gaseous flames with isolated ethanol droplet injection. The evidence for the local extinction on the flame surface due to droplet passage was found via the Chemiluminescence method. The intrinsic instabilities were found to be triggered by the droplets in cases where the flame cannot recover its initial state.

Keywords. Two-phase combustion, cellular instabilities, local extinction, droplet-flame interaction, flame morphology, laminar flames.

Funding. The first author is supported by French Government Cotutelle Scholarship for her joint PhD studies between METU & Université d'Orléans and TÜBİTAK BİDEB 2211-C Scholarship.

Published online: 6 April 2023

* Corresponding author.

1. Introduction

Spray combustion occurs in various combustion applications, i.e., internal combustion engines, gas turbine combustion, liquid-fueled rockets, and burners. In these applications, strong spray/combustion interactions occur in the combustion chamber resulting in higher flame propagation speeds and flame instabilities compared to the gaseous flame at the same conditions [1–5].

Many experimental, theoretical, and numerical studies have been conducted to characterize the evaporation and combustion of droplets and their effects on a gaseous flame in different configurations. One of these configurations includes the presence of mono-sized and mono-dispersed droplet clouds due to the resemblance of spray combustion. Burgoyne and Cohen conducted the first study on mono-dispersed liquid aerosol flame with tetralin having 7-55 μm droplet size. [1]. They concluded that a brush-like flame structure was observed for the droplets larger than 10 μm. Mizutani and Nakjima reported that small kerosene droplets increased the burning velocity of propane more for lean flames than rich flames [2]. Hayashi and Kumagai used the Wilson cloud chamber method [6] to generate mono-sized droplets in a stagnant mixture [7, 8]. They created ethanol droplets with nearly 7 and 20 μm mean droplet sizes and reported that cellular flames were observed under microgravity at rich conditions for sufficiently large diameters. At the same time, the burning velocity increased under lean conditions. Atzler and co-workers also studied possible mechanisms of flame instabilities for iso-octane aerosol flames [9]. Their findings resulted in the observation of cellular instabilities with an increase in flame surface area and burning rate due to the change in the local equivalence ratio. Lawes et al. reported similar observations under microgravity conditions for iso-octane droplets [10]. Bradley et al. also observed flame surface wrinkling resulted in Darrieus–Landau and thermo-diffusive instabilities due to the presence of large alcohol droplets, which may enter the reaction zone and significantly increase the fuel mass flux [11]. Thimothée et al. demonstrated that the gaseous ethanol-air flame was stable and smooth, as well as the aerosol flame with ethanol droplets fully vaporized in the pre-heating zone [12]. They also suggested a possible mechanism leading to the instabilities, including the heat sink phenomenon due to the heat taken by the droplet for vaporization from the flame field using water droplets as an inert medium [13]. They also correlated the topology of instabilities with the evaporation characteristics at different conditions under microgravity [14]. Renoux and co-workers extended the investigation under similar conditions by reporting a stability envelope for rich ethanol aerosol flames [15]. Spray-induced instabilities resulted from the perturbations on the flame front via surface area increase due to droplet passage.

Many studies mentioned above focused on the effect of liquid droplets on the flame propagation speed and morphology experimentally. In order to foresee the initiation of the change in flame parameters and structure, heat sink and local extinction phenomena are studied by many researchers for the interaction of the droplet and flame. Greenberg and co-workers theoretically predicted the onset of instabilities due to the heat loss from the flame zone for the evaporation of droplets via linear stability analysis [16, 17]. They reported that for richer conditions, droplets caused an increase in surface area and burning velocity while creating a heat sink, resulting in cellular structures [18]. They also developed an approach to understand how the amount of liquid fuel and the latent heat of vaporization affected the onset of instabilities causing flame extinction [19]. Han and co-workers also theoretically studied the sensitivity of spherical flame propagation and ignition to the finite rate of evaporation [20, 21]. They concluded that the flame structure was affected by droplet evaporation only by the heat absorbed for rich conditions. In contrast, local equivalence ratio change also had an impact on lean conditions. Recently, Li et al. reported the effects of heat loss from the flame to droplet for evaporation and Lewis number on

laminar planar flame propagation under droplet mists [22]. It was observed that for highly evaporative droplets, the flame propagation speed was decreased due to the heat sink on the flame zone [23]. Finally, numerical studies were performed by Nicoli and co-workers by performing DNS simulations of flame propagation in the presence of water droplets [24] and compared with microgravity experiments [25]. For larger droplet inter-distance, they reported the quenching in the flame zone due to the presence of water droplets, leading to the observation of Darrieus–Landau instabilities.

In the previous studies, the evidence of cellular instabilities caused by the presence of droplets was reported under microgravity conditions for aerosol ethanol flames via several optical diagnostics [12–15, 25–28]. However, there are very few experimental studies of the single droplet effect on the flame instabilities. In this study, the analogy between the aerosol flame and gaseous flame with a single droplet is investigated in order to understand the local extinction phenomenon resulting in flame instabilities. First, a qualitative analysis is performed from Schlieren images obtained in a zero-g environment at well-known and repeated conditions, reported by Renoux and co-workers [15], for spherically-expanding rich aerosol ethanol/air flames. Then, from the observation of the formation of local sinks and holes at the beginning of the cellular structures, the evidence of the local extinction phenomenon is investigated for rich propane/air gaseous stagnation flames at ground conditions with an isolated ethanol droplet injection.

2. Experimental

2.1. *Microgravity experiments: Spherically-expanding aerosol flame*

Microgravity experiments were performed during the parabolic flights of CNES Airbus A310 ZERO-G flight with aerosol spherical chamber configuration, given in Figure 1 (a), in order to observe cellular instabilities on the flame front due to the presence of droplets.

The experimental setup consists of two pressure-release-type chambers; an inner combustion chamber with 1 L volume and an outer high-pressure chamber with 11 L volume. The inner and outer chambers were filled with a premixed mixture and nitrogen for each experiment, respectively. There are eight evacuation valves inside the combustion chamber to evacuate the pressurized gases to the high-pressure chamber during the combustion to prevent the sudden release of pressure in the combustion chamber thanks to the high volume ratio between outer and inner chambers.

At the beginning of each set of experiments, the inner chamber was vacuumed and then filled with dry air and evaporated fuel via mass flow meters at the desired equivalence ratio and initial pressure. The amount of liquid fuel is adjusted with a liquid pump. Then, the fuel was fed to the preheater before feeding to the combustion chamber.

The fuel aerosol was created via the Wilson cloud chamber principle [29] by decreasing the pressure in the combustion chamber with the connection to an 0.5 L expansion vessel, leading to a temperature drop and finally, the condensation of the fuel. Thanks to the zero-g environment, mono-sized, uniformly distributed droplets could be maintained systematically inside the combustion chamber without settling to the bottom of the chamber. Then, the heterogeneous mixture was ignited via tungsten electrodes at the chamber's center. The distance between droplets, number of droplets, and droplet size was controlled by thermodynamic parameters such as initial pressure, $P_i = P_{ignition} + \Delta P$, equivalence ratio, ϕ, pressure drop, ΔP and duration of pressure drop, reported in Table 1 below. More details on the principle of aerosol creation can be found in the previous studies [12–15, 25–28].

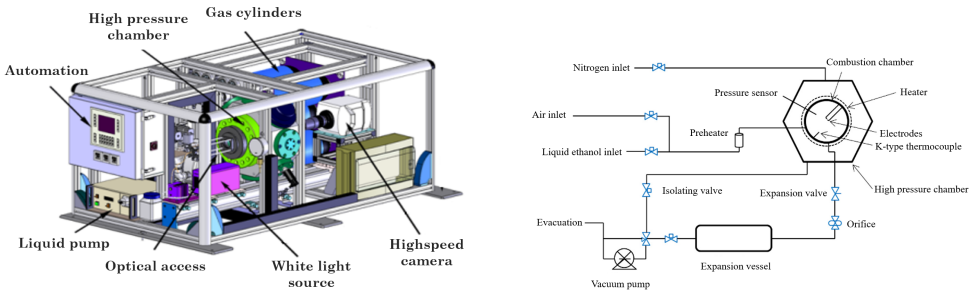

(a) (b)

Figure 1. (a) Experimental setup with Schlieren configuration. (b) The schematic of the aerosol chamber (AC).

The experimental configuration is presented in Figure 1. The combustion chamber was coupled with a laser-driven white light source (Energetiq LDLS 170 nm-2100 nm) and a high-speed camera, Phantom v1210 equipped with Nikon AF Micro-NIKKOR 105 mm lens. For imaging, 10,000 frames/s rate was used.

Experiments were performed with ethanol, C_2H_5OH as fuel and dry air (80% N_2, 20% O_2) at the conditions presented in Table 1 below. These conditions have been repeated in the previous studies by Renoux et al. [15, 26], and the characterization of the liquid phase has been done via several optical diagnostics. Therefore, the same droplet properties are assumed to be valid for this study.

Table 1. Experimental conditions performed in the aerosol chamber (AC) for spherically-expanding aerosol C_2H_5OH/air flames

Condition	$P_{ignition}$ (MPa)	ϕ	ΔP (MPa)	$T_{ignition}$ (K)	a_{mean} (mm)	SMD (μm)	δ_L (mm)	Le_{eff}
AC-1	0.25	1.2	0.15	337	0.527±0.05	9.8±0.9	0.21	1.12
AC-2	0.33	1.3	0.12	341	0.596±0.05	8.3±0.9	0.19	1.10
AC-3	0.33	1.4	0.12	341	0.538±0.05	8.7±0.9	0.24	1.04
AC-4	0.30	1.1	0.20	339	0.497±0.05	9.9±0.9	0.18	1.19
AC-5	0.30	1.2	0.20	339	0.502±0.05	9.9±0.9	0.21	1.08
AC-6	0.35	1.0	0.25	335	0.468±0.05	9.6±0.9	0.18	1.31

2.1.1. *Optical diagnostics*

Schlieren technique was used to visualize the flame morphology for microgravity experiments. Two pairs of aligned transparent windows achieve optical access for the chamber. Two spherical lenses were replaced on the back and front of the chamber so that the light could penetrate as a sheet. In order to track the cellular structure, the distance between lenses was adjusted so that the darkness would be at the minimum level. Before the high-speed camera, a pinhole with a diameter of 0.7 mm was placed to focus the light.

During the parabolic flight, the pinhole was too sensitive to the changes in gravitational acceleration, and the opening was moved while g was changing. This situation caused unwanted darkness and visualization loss at several experimental conditions. Therefore, Schlieren images

are only used to obtain qualitative interpretations for the formation mechanisms of instabilities for the sake of certainty.

2.2. *Ground experiments: Stagnation flame*

Ground experiments were performed with a stagnation burner, given in Figure 2 (a), to observe the local extinction phenomenon due to the droplet passage through the flame front. Flame stabilization was achieved thanks to N_2 co-flow and the presence of an upper stagnation plate located 25 mm away from the burner outlet. A premixed mixture of air and fuel was fed to the system, and the mixture was ignited with an external igniter in the region between the stagnation plate and the burner outlet. Monodispersed isolated ethanol droplets with around 50 μm diameter were generated by a piezoelectric injector (Microdrop Technologies MDK-140). The frequency of the droplet injection was adjusted accordingly so there could not be any coagulations and close-distance droplets generated. The droplets were injected perpendicularly to the flame zone through a needle in which premixed gases carry them. The schematic of the stagnation burner is given in Figure 2 (a). Details of the stagnation flame burner can also be found in other studies [30], [26].

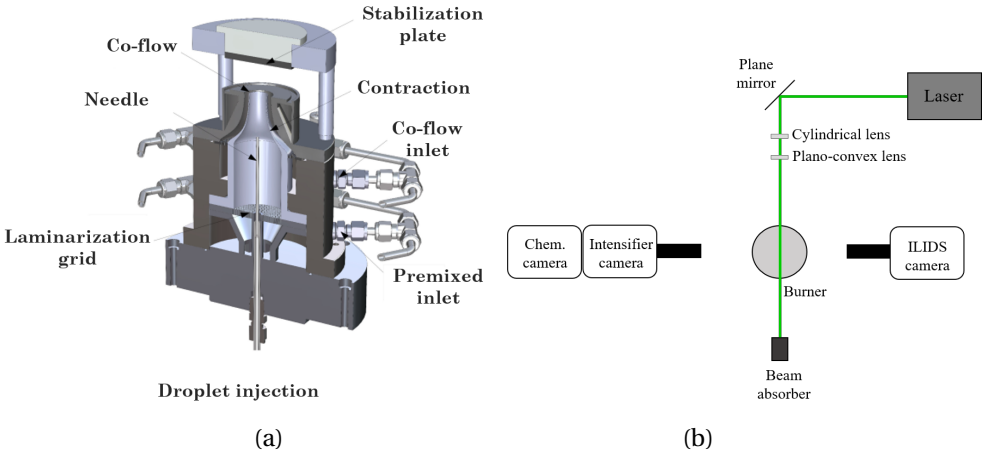

Figure 2. (a) The schematic of the stagnation burner (SB) [31]. (b) Experimental configuration with ILIDS and Chemiluminescence.

Experimental configuration is represented in Figure 2 (b). The stagnation burner was coupled with a laser device, Coherent Verdi emitting at 532 nm, and a 2D laser sheet was created from a continuous laser beam with the help of one semi-cylindrical divergent lens (f2 = -25 mm) and one plano-convex lens (f2 = 500 mm). Two high-speed cameras, in addition to an intensifier, were used for visualization. The first camera, Phantom v1210 equipped with Sigma APO Macro 180 mm lens at the maximum opening, was utilized to measure the initial droplet size via ILIDS (Interferometric Laser Imaging for Droplet Sizing). A second camera, Phantom v1611 equipped with Sigma APO Macro 180 mm lens at the maximum opening, 38 mm extension system and 1:1 2x magnifier, was coupled with La Vision High-Speed IRO with 90 μs gate, in order to observe the changes in the flame front due to the droplet passage via Chemiluminescence. The cameras for ILIDS and Chemiluminescence had the same frame rate of 10,000 images per second. The camera acquisition sequence was triggered by a common trigger signal to align both cameras

and the intensifier in the time frame. 13.7 μm/px and 27.3 μm/px resolutions were obtained for Chemiluminescence and ILIDS cameras, respectively.

In this part of the study, experiments were performed with ethanol droplet as the liquid fuel and C_3H_8/air premixed gaseous flames at fuel-rich conditions, reported in Table 2 below.

Table 2. Experimental conditions performed in the stagnation burner (SB) for C_3H_8/air premixed stagnation flames with an ethanol droplet

Condition	ϕ	d_0 (μm)	δ_L (mm)	Le_{eff}
SB-1	1.4	48.5	0.61	1.14
SB-2	1.3	51.9	0.46	1.18
SB-3	1.2	58.9	0.40	1.24
SB-4	1.1	55.4	0.39	1.31

2.2.1. *Optical diagnostics and image processing*

Interferometric Laser Imaging for Droplet Sizing (ILIDS) is utilized to obtain the initial droplet size. The high-speed camera used for ILIDS allows a good temporal resolution for the evolution of the droplet size by defocusing and capturing the interference fringe pattern of the droplet at each frame. By providing a high laser power, it is possible to increase the detection of fringes even if the droplet size is minimal since the ILIDS method is based on the reflected and the refracted rays visible on the droplet surface. In this study, 6 Watts laser power was used, enough to detect the droplet before reaching the flame zone. The number of fringes is computed for an individual droplet based on Discrete Fourier Transform (DFT) on the five vertical sections of the fringe pattern. With the help of peak intensities in Fourier space, the fringes is detected and computed. The fringe pattern for a droplet before reaching the flame zone is illustrated in Figure 3.

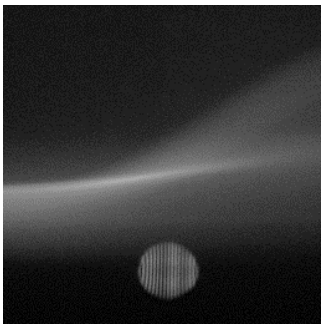

Figure 3. ILIDS image illustrating the droplet with 59 μm diameter injected to the flame front

The droplet diameter based on the number of fringes is then calculated from the following relation [15];

$$d = N_{fringe}\frac{2\lambda}{\alpha}\left[cos(\theta/2) + \frac{m\,sin(\theta/2)}{\sqrt{m^2 - 2\,m\,cos(\theta/2) + 1}}\right]^{-1} \tag{1}$$

where d is the particle diameter, N_{fringe} is the number of fringes on the droplet, θ is the scattering angle (here, 90°), α is the collecting angle, λ is the laser wavelength (here, 532 nm) and m is the refractive index of the droplet. In this configuration, 3.46 μm/fringe resolution is obtained.

In order to observe the structural changes in the flame front, ILIDS is coupled with the flame luminosity measurements, Chemiluminescence. Direct measurement of the luminosity, which corresponds to the CO_2 radiation, is performed instead of using special band filters. It is known that with Chemiluminescence measurement, the integral signal along the sight of the line is captured, making it hard to observe small surface changes. The fuel was selected as propane and the high luminosity of propane can be captured by an intensifier with a low noise ratio so that the surface modifications can be captured during the post-processing of images. Chemiluminescence image of C_3H_8/air flame at ϕ =1.3 is given in Figure 4.

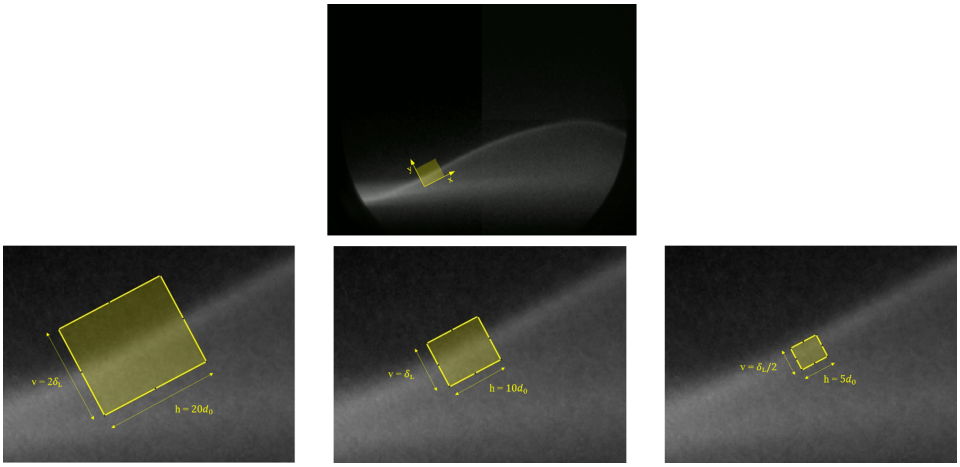

Figure 4. Chemiluminescence image of C_3H_8/air flame at ϕ =1.3 with the region of interest (yellow) having different sizes depending on the flame thickness and initial droplet size

The local extinction phenomenon is investigated from Chemiluminescence images by creating a region of interest (ROI) in the droplet passage zone, as seen from Figure 4. The dimensions of the ROI are adjusted so that the horizontal distance is 20, 10, and 5 times the initial droplet size, d_0 and the vertical distance is 2, 1, and 0.5 times the flame thickness, δ_L. The ROI is also rotated by 28° to capture the signal loss from the perpendicular region to the flame. Two approaches are followed for region selection:

(1) The position of the ROI is kept constant at each frame.
(2) The position of the ROI is updated at each frame by changing its center according to the flame position. The flame position is updated for each image by calculating the position of the maximum intensity along a perpendicular line to the flame (y-axis) due to the fact that the flame oscillates slightly during the experiments. Then, the ROI is moved along the y-axis so that its center is aligned with the flame along the x-axis.

After positioning the ROI, the integral of the signal is computed for this region at each frame since it is expected to see a decrease in the signal when the droplet passes the flame zone. This phenomenon is also known as the local extinction phenomenon.

3. Results and Discussions

3.1. *Cellular instabilities on aerosol flame*

Renoux et al. performed the same experimental conditions, given in Table 1, with Mie scattering to determine the droplet position and inter-distance, with ILIDS to compute the droplet size and

with Shadowgraphy and Chemiluminescence to observe the flame morphology [15]. In this study, the morphology of the flame was determined via Schlieren method. In Figure 5, the comparison between Shadowgraphy, Chemiluminescence, and Schlieren images at the same condition are given. From these images, it can be interpreted that aerosol creation is successfully achieved, and the droplets are observed inside the combustion chamber without settling under a zero-g environment. While during the experiments of Renoux and co-workers (Figure 5 (a) and (b), homogeneous distribution of the droplets is observed, Schlieren image indicates that most of the droplets are near the top right corner of the chamber. This can be explained due to the movement of the plane, resulting in the movement of the droplets towards this side. Still, cellular structures can easily be observed under the reported conditions for qualitative interpretations.

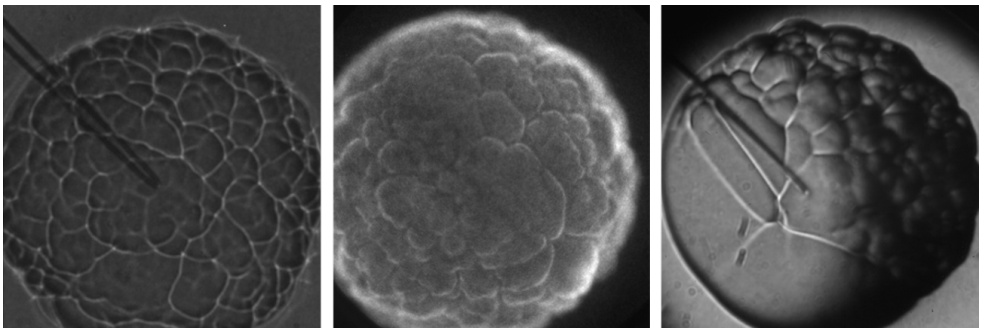

(a) (b) (c)

Figure 5. Comparison of (a) Shadowgraphy [15], (b) CH* Chemiluminescence [15] and (c) Schlieren images of equivalent flames and at a radius of 13.5 mm (aerosol ethanol/air flame at AC-1).

It is obviously seen that Shadowgraphy provides the clearest images for cell size detection. Renoux and co-workers reported the cell size distribution and stability envelope based on these images. However, as it is seen in Figure 5 (c), cell sizes are hard to detect with Schlieren method due to the sensitivity of the pinhole to the changes in gravitational acceleration during parabolic flight, resulting in shadows and darkness with a fixed position at the certain zones of the combustion chamber. Nevertheless, Schlieren method provides an additional information for the initiation of these cells, as it is the measurement of the first derivative of the flame field. In Figure 6, snapshots of the propagating flame can be seen in time for the condition of AC-1.

By focusing the wrinkles, first, the dark spots are observed, as in t=8.1 ms, indicating the loss of signal in the density gradient of the flame. Then, the extension of the flame surface can be seen as a lighter zone corresponding to the cellular cell formation. The dark spots and signal loss at the initiation of instabilities can be interpreted as the local hole structures due to the passage of liquid droplets and quenching in the flame zone, leading to the formation of the edges of cells. The same mechanism is observed for all performed conditions.

As pointed out in Renoux and co-worker's results, the droplets only act as a trigger on the development of the instabilities due to the fact that the wavenumbers related to droplet inter-distance are higher than the mode wavenumbers [15]. These instabilities then lead to intrinsic instabilities on gaseous flame. Therefore, it can be interpreted that the droplets act as obstacles that absorb heat from the flame zone for evaporation and cause local extinction on the flame surface by changing the flame properties locally.

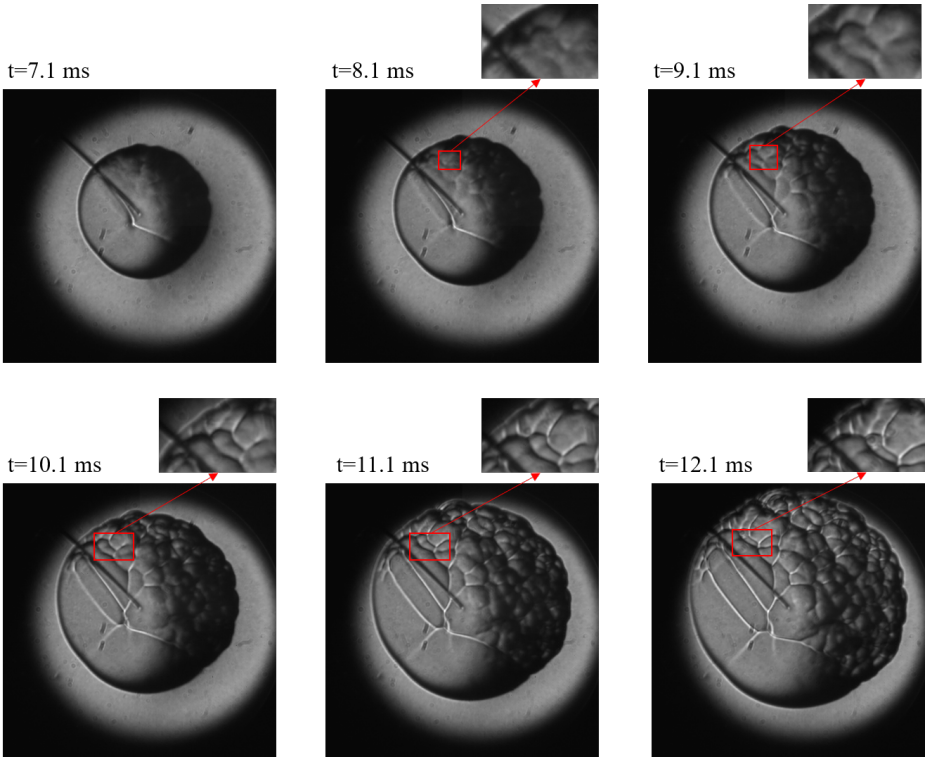

Figure 6. Formation of instabilities on the flame surface due to the presence of droplets (aerosol ethanol/air flame at AC-1).

3.2. *Local extinction due to droplet passage on stagnation flame*

The stagnation flame configuration with an isolated droplet injection is found to be very suitable for simplifying the physics and understanding the local extinction phenomenon deeply. These experiments were performed with a propane/air gaseous flame due to its high luminosity. Moreover, the Lewis number is slightly higher than the unity for rich propane/air flames, which tend to be prone to cellularities induced both by hydrodynamic and thermo-diffusive instabilities. Therefore, these flames are chosen to be good candidates for sensitivity to droplet passage. It is worth mentioning that the amount of premixed gas fed from the droplet injection tube was increased to create a flame surface with a little bump in order to increase the possibility of capturing the decrease in signal at the droplet injection point. It was done due to the fact that the camera captures the signal from the flame as a line integral of signals. Hence, if the signal is distributed to more areas, it will be easier to distinguish any change in a specific region. Since the curvature is negligible, the flame surface is still treated as flat.

The evaporation of an isolated ethanol droplet was investigated previously under premixed methane/air flame conditions, and it is found that 50 μm diameter is high enough to cross the flame front under elevated temperatures, regardless of the gas composition [30]. Hence, the droplet passage through the flame field and its effects on the flame structure can properly be observed under the fixed conditions, reported in Table 2. Additionally, Chemiluminescence experiments also showed that for fuel-rich propane/air flames, a perturbation occurs on the flame surface after the droplet passage. This perturbation, first, propagates with an increasing amplitude and then vanishes towards the edge of the flame. However, unlike spherically-expanding flames

at the similar flame conditions, the stagnation flames preserve its stable structure after a certain time from the droplet passage.

First, the decrease in collected signal from the flame surface when the droplet passes is computed. In order to achieve this, the summation of pixel values inside a specified region is calculated with two different approaches; with a constant position region of interest, given in Figure 7 and with an adaptive region of interest along with the flame position, shown in Figure 8 for ϕ=1.4 with d_0=48.5 μm. Although the decrease in the signal can be detected with both approaches, it is hard to distinguish from the former one due to the fact that the flame is oscillating during the experiment. Therefore, the adaptive approach is more suitable for capturing the percentage signal loss during the droplet passage since the baseline can be drawn to the flame position. For the adaptive ROI calculations, the total signal amount is normalized so that all cases can be compared.

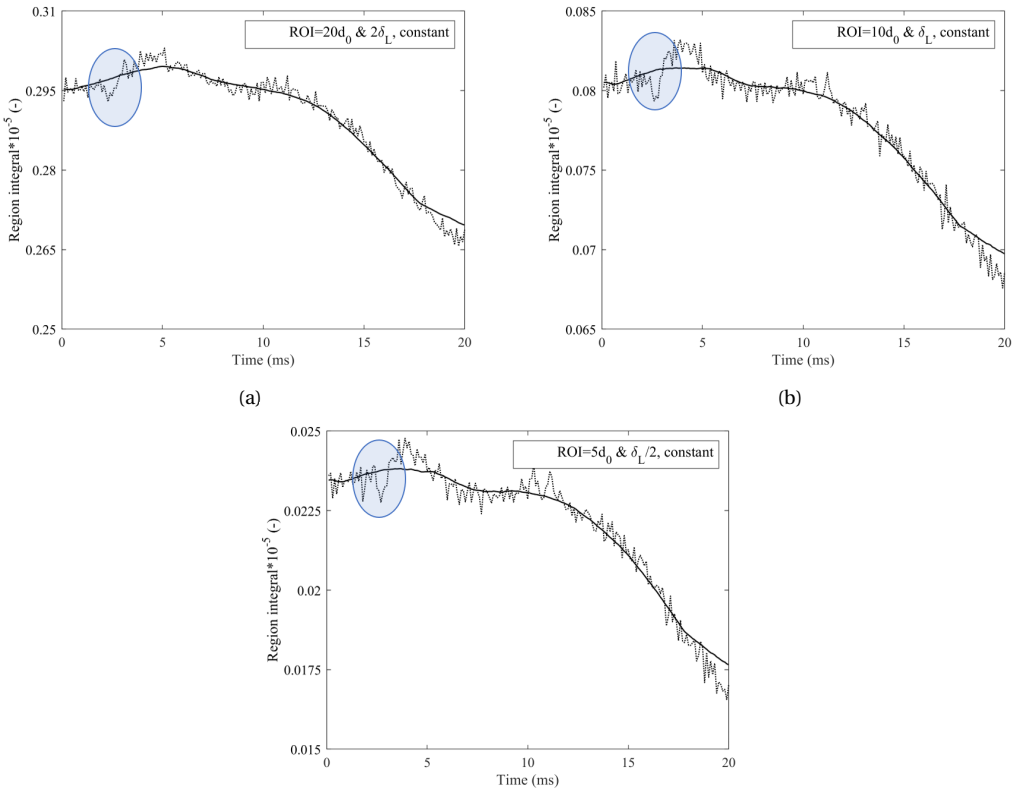

Figure 7. Change in integral of signal due to droplet passage (d_0=48.5 μm) at SB-1 with constant position ROI.

As it can be seen from Figure 8, the decrease in signal is observed between 2 to 6.6 ms, and the flame is recovered after the droplet passage. The decrease in the signal can directly be related to the droplet-flame interaction, where the droplet losses its mass due to evaporation. Since the fuel-rich cases do not contain excess oxygen in the flame zone, the droplet will not be oxidized. Hence, as the droplet takes heat from the flame, the luminosity and reactivity of the flame will decrease. For the droplet having 48.5 μm initial diameter, this time takes 1.7 ms. The recovery time takes almost 4.9 ms, which also depends on flame properties and the droplet's initial diameter and evaporation constant. The normalized signal values indicate 12%, 13.2%, and

15% signal loss during the droplet passage for the corresponding region of interest dimensions. For the smallest ROI, post-processing needs to be more accurate on the first detection of droplet passage so that the interaction point needs to be in the middle of the rectangle. Since the signal loss is very high compared to leaner cases, it can easily be determined for ϕ=1.4, which has the highest luminosity among the reported cases.

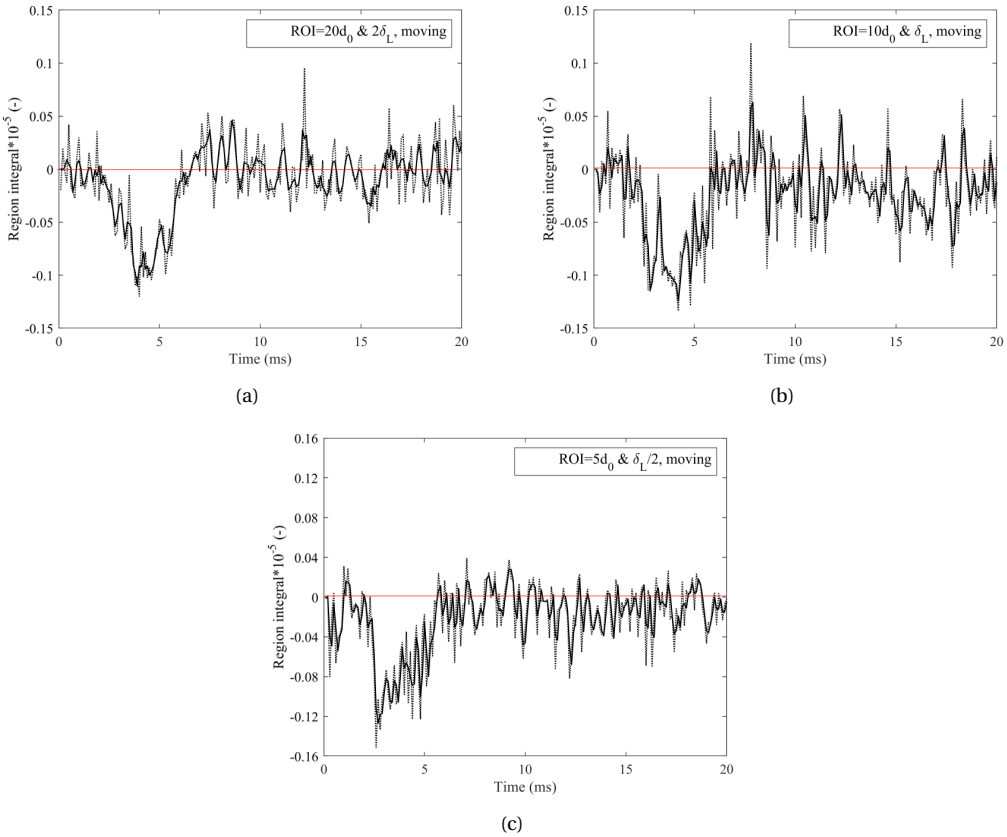

Figure 8. Change in integral of signal due to droplet passage (d_0=48.5 μm) at SB-1 with moving ROI.

Similar conclusions can be drawn for ϕ=1.3 in Figure 9, in which an average 10.71 % signal loss is detected between 2.2-5.5 ms. The recovery time for the flame, nearly 1.9 ms, is less than the richest case because when the flame condition is closer to stoichiometry, the flame is less prone to disturbances. Although the initial droplet diameter is slightly higher in SB-2 than in SB-1, heat loss duration differs by 0.3 ms due to the increased flame temperature, resulting in quicker evaporation.

At ϕ=1.2, the detection for signal loss can only be captured with the large ROI as 5.1 % on average during 3.6 ms, as given in Figure 10. The recovery time after extinction is calculated as 2.9 ms while the droplet crossing time is 0.7 ms, even though it is the largest droplet injected. The flame temperature for this case is nearly 75 K higher than ϕ=1.3 so that the droplet will evaporate more inside the preheating and reaction zones. As a result, gaseous ethanol will build up near to flame region, leading to more time to recover the flame itself.

In Figure 11, total signal inside ROI is given for ϕ=1.1. As can be seen clearly, it is almost impossible to detect signal loss with an adaptive ROI. However, from global computations, 1.8 %

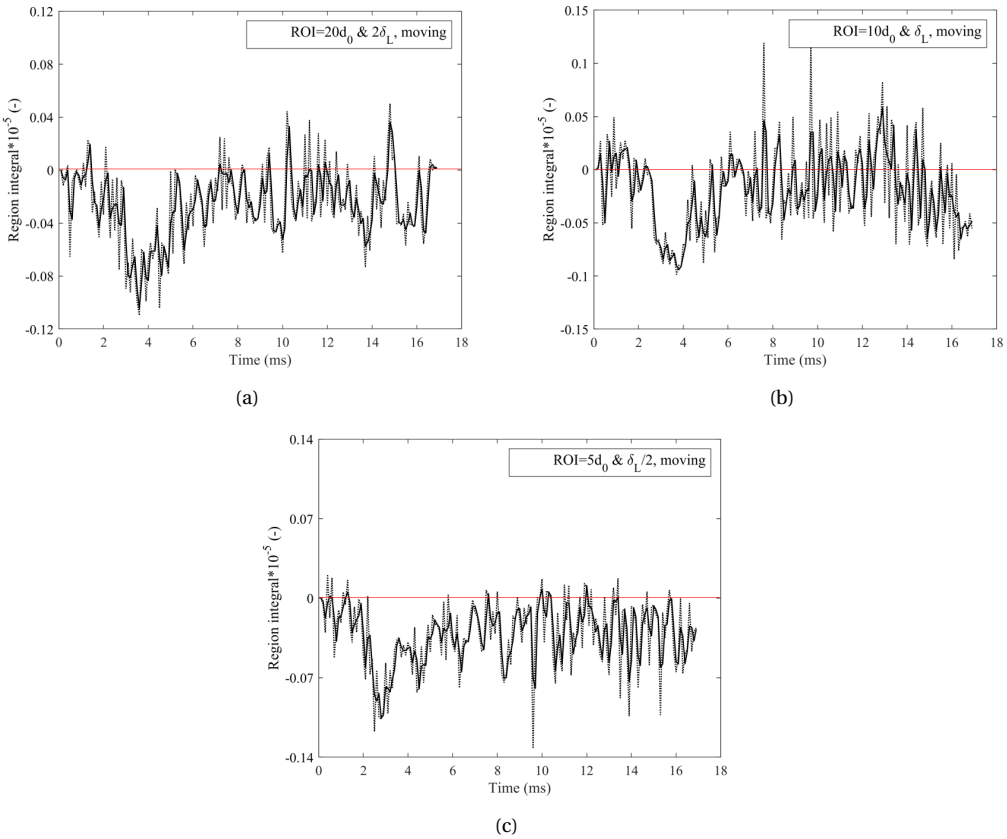

Figure 9. Change in integral of signal due to droplet passage (d_0=51.9 μm) at SB-2 with moving ROI.

signal loss can be reported for 0.5 ms. For near-to-stoichiometric cases, it is hard to distinguish the signal with a smaller region of interest. The first reason is that the luminosity of the flame will decrease when it becomes leaner. Secondly, leaner flames will be more stable, and they will be less sensitive to any changes.

In light of these results, the onset of instabilities and the effect of droplet passage from the flame surface are investigated. The reactive droplet takes heat from the flame front while passing, evaporating, and possibly burning, depending on the flame condition. This leads to local quenching on the flame zone. For fuel-rich propane/air flames, there is enough time for the flame to recover itself. However, for spherically-expanding aerosol ethanol/air flames, due to a high number of droplets with a small inter-distance, the flame surface will continually be disturbed without any time for recovery. Due to the evaporation of liquid fuel, the gaseous phase will be fed with more fuel thanks to the evaporated gas around the droplet. This concentration gradient locally changes the properties of flame, i.e., temperature, velocity, and diffusivity. The build-up of evaporated fuel may also cause an aperture on the flame field, which may lead to instabilities. The intrinsic instabilities are triggered by the presence of droplets in the cases where the flame cannot recover its initial state, and it locally extincts due to the heat sink effect from the presence of droplets, as observed for spherically-expanding flames. Additionally, the richer flames are more prone to local modifications, hence the recovery time is higher than the leaner flames.

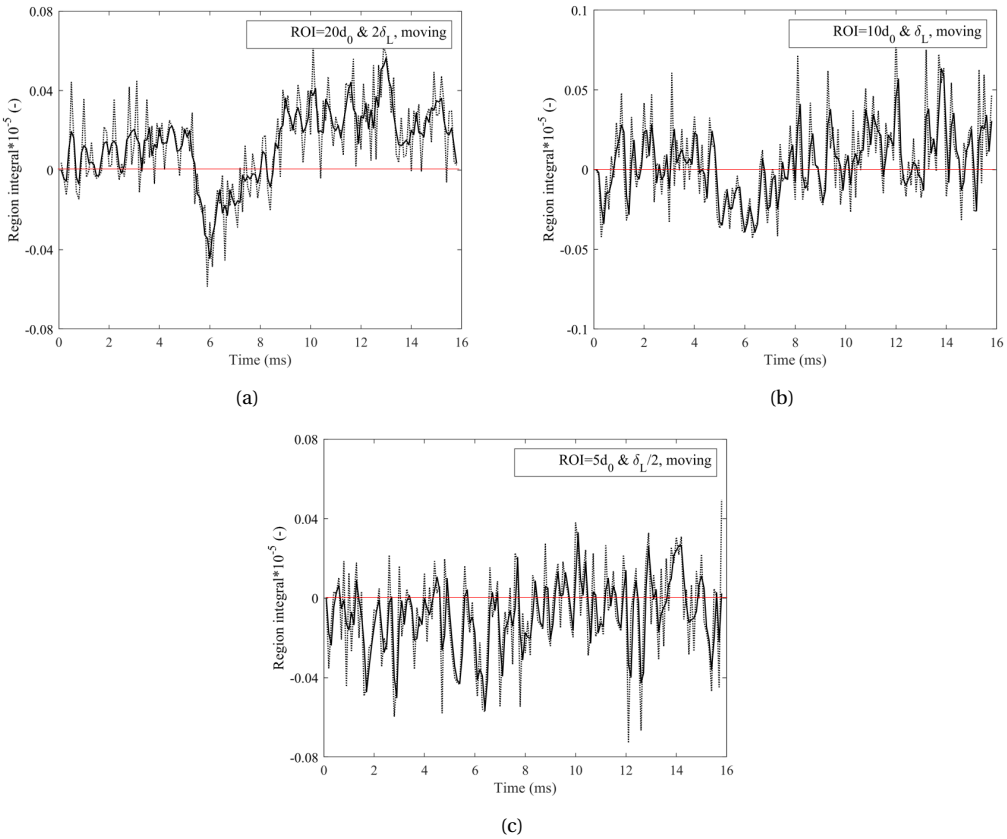

Figure 10. Change in integral of signal due to droplet passage (d_0=58.9 μm) at SB-3 with moving ROI.

4. Conclusion

The main purpose of this study is to investigate the flame/spray interactions. Accordingly, mechanism of cellular instability formation and the link between instabilities and local extinction are studied. In the first part of the study, spherically-expanding aerosol ethanol/air flame morphology is observed under microgravity via Schlieren method at well-established and reported conditions. Schlieren images revealed that at the initial phase of cellular structure formation, dark spots are observed linking to the signal loss in a density gradient. This phenomenon leads to a local extinction and quenching on the flame front due to either the presence or the evaporation of liquid droplets.

For further investigation of local extinction phenomenon, stagnation flame with a single droplet injection is examinated in the second part of the study. Rich propane/air flames are selected due to their high luminosity and sensitivity to disturbances, and their structure is captured via Chemiluminescence method. The droplet is selected as ethanol and tracked via ILIDS to determine its initial size. It is observed that the percentage signal loss due to the droplet passage is higher for richer cases, as well as the recovery time of the flame surface. The detection of signal loss can be achieved by changing the dimensions of the region of interest for richer cases. However, it is hard to detect the signal loss when the flame is close to the stoichiometry since it is less prone to disturbances. Although all the flames created at both flame configurations

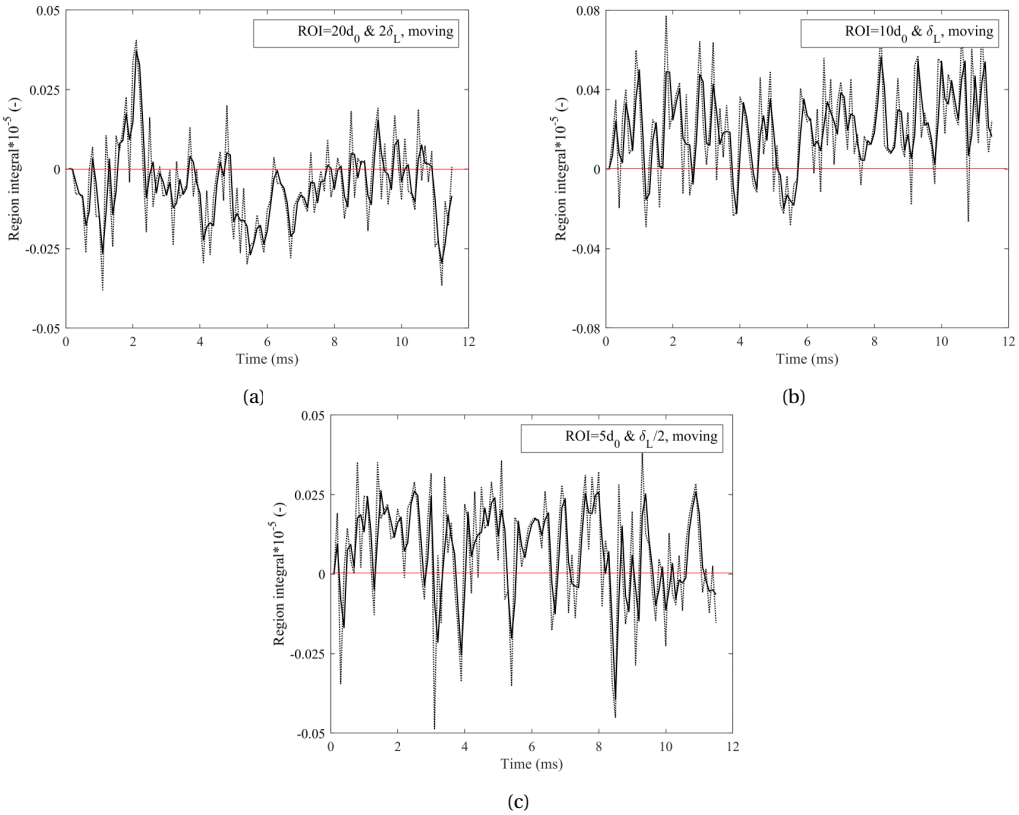

Figure 11. Change in integral of signal due to droplet passage (d_0=55.4 μm) at SB-4 with moving ROI.

are tend to be stable, the intrinsic instabilities are only triggered by droplets if the flame front is continuously fed with them, which is the case in spherically-expanding aerosol flames.

Conflicts of interest

The authors have no conflict of interest to declare.

Acknowledgments

The authors acknowledge CNES and CNRS for their financial and technical support for the parabolic flights.

References

[1] J. H. Burgoyne, L. Cohen, “The effect of drop size on flame propagation in liquid aerosols”, *Proc. R. Soc. Lond., Ser. A* **225** (1954), no. 1162, p. 375-392.

[2] Y. Mizutani, A. Nakajima, “Combustion of fuel vapor-drop-air systems: Part II—Spherical flames in a vessel”, *Combust. Flame* **20** (1973), no. 3, p. 351-357.

[3] D. R. Ballal, A. H. Lefebvre, “Flame propagation in heterogeneous mixtures of fuel droplets, fuel vapor and air”, *Symposium (International) on Combustion* **18** (1981), no. 1, p. 321-328.

[4] G. D. Myers, A. H. Lefebvre, "Flame propagation in heterogeneous mixtures of fuel drops and air", *Combust. Flame* **66** (1986), no. 2, p. 193-210.

[5] H. Nomura, K. Izawa, Y. Ujiie, J. Sato, Y. Marutani, M. Kono, H. Kawasaki, "An experimental study on flame propagation in lean fuel droplet-vapor-air mixtures by using microgravity conditions", *Symposium (International) on Combustion* **27** (1998), no. 2, p. 2667-2674.

[6] C. T. R. Wilson, "On a method of making visible the paths of ionising particles through a gas", *Proc. R. Soc. Lond., Ser. A* **85** (1911), no. 578, p. 285-288.

[7] S. Hayashi, S. Kumagai, "Flame propagation in fuel droplet-vapor-air mixtures", *Symposium (International) on Combustion* **15** (1975), no. 1, p. 445-452.

[8] S. Hayashi, S. Kumagai, T. Sakai, "Propagation velocity and structure of flames in droplet-vapor-air mixtures", *Combust. Sci. Technol.* **15** (1977), p. 169-177.

[9] F. Atzler, F. X. Demoulin, M. Lawes, Y. Lee, N. Marquez, "Burning rates and flame oscillations in globally homogeneous two-phase mixtures (flame speed oscillations in droplet cloud flames)", *Combust. Sci. Technol.* **178** (2006), no. 12, p. 2177-2198.

[10] M. Lawes, Y. Lee, N. Marquez, "Comparison of iso-octane burning rates between single-phase and two-phase combustion for small droplets", *Combust. Flame* **144** (2006), no. 3, p. 513-525.

[11] D. Bradley, M. Lawes, S. Liao, A. Saat, "Laminar mass burning and entrainment velocities and flame instabilities of i-octane, ethanol and hydrous ethanol/air aerosols", *Combust. Flame* **161** (2014), no. 6, p. 1620-1632.

[12] R. Thimothée, C. Chauveau, F. Halter, I. Gökalp, "Characterization of cellular instabilities of a flame propagating in an aerosol", in *Proceedings of ASME Turbo Expo 2015: Turbine Technical Conference and Exposition*, American Society of Mechanical Engineer, 2015.

[13] R. Thimothée, C. Chauveau, F. Halter, I. Gökalp, "Experimental investigation of the mechanisms of cellular instabilities developing on spherical two-phase flames", *Combust. Sci. Technol.* **188** (2016), no. 11-12, p. 2026-2043.

[14] R. Thimothée, C. Chauveau, F. Halter, I. Gökalp, "Experimental investigation of the passage of fuel droplets through a spherical two-phase flame", *Proc. Combust. Inst.* **36** (2017), no. 2, p. 2549-2557.

[15] G. Renoux, F. Halter, C. Chauveau, "Experimental study of the morphology of two-phase flame instabilities in microgravity", *At. Sprays* **28** (2018), no. 10, p. 915-929.

[16] J. B. Greenberg, A. McIntosh, J. Brindley, "Instability of a flame front propagating through a fuel-rich droplet–vapour–air cloud", *Combust. Theory Model.* **3** (1999), no. 3, p. 567-584.

[17] J. B. Greenberg, "Propagation and extinction of an unsteady spherical spray flame front", *Combust. Theory Model.* **7** (2003), p. 163-174.

[18] J. B. Greenberg, A. C. McIntosh, J. Brindley, "Linear stability analysis of laminar premixed spray flames", *Proc. R. Soc. Lond., Ser. A* **457** (2001), no. 2005, p. 1-31.

[19] J. B. Greenberg, "Finite-rate evaporation and droplet drag effects in spherical flame front propagation through a liquid fuel mist", *Combust. Flame* **148** (2007), no. 4, p. 187-197.

[20] W. Han, Z. Chen, "Effects of finite-rate droplet evaporation on the ignition and propagation of premixed spherical spray flame", *Combust. Flame* **162** (2015), no. 5, p. 2128-2139.

[21] W. Han, Z. Chen, "Effects of finite-rate droplet evaporation on the extinction of spherical burner-stabilized diffusion flames", *Int. J. Heat Mass Transfer* **99** (2016), p. 691-701.

[22] Q. Li, H. Zhang, C. Shu, "Propagation of heterogeneous and homogeneous planar flames in fuel droplet mists", *Int. J. Multiphase Flow* **133** (2020), article no. 103452.

[23] Q. Li, H. Zhang, C. Shu, "Propagation of weakly stretched premixed spherical spray flames in localized homogeneous and heterogeneous reactants", *Phys. Fluids* **32** (2020), article no. 123302.

[24] C. Nicoli, P. Haldenwang, B. Denet, "Premixed flame dynamics in presence of mist", *Combust. Sci. Technol.* **191** (2019), no. 2, p. 197-207.

[25] R. Thimothée, C. Chauveau, F. Halter, C. Nicoli, P. Haldenwang, B. Denet, "Microgravity experiments and numerical studies on ethanol/air spray flames", *C. R. Méc. Acad. Sci. Paris* **345** (2017), no. 1, p. 99-116.

[26] G. Renoux, "Étude expérimentale de l'interaction goutte/flamme : propagation d'une flamme dans un aérosol en microgravité et passage d'une goutte à travers un front de flamme", PhD Thesis, Université d'Orléans, Orléans, France, 2020.

[27] R. Thimothée, "Caractérisation de la propagation d'une flamme dans un milieu diphasique (brouillards) en microgravité", PhD Thesis, Université d'Orléans, Orléans, France, 2017.

[28] M. Nassouri, "Caractérisation expérimentale de la propagation d'une flamme laminaire dans un milieu diphasique (brouillard) à haute pression et en microgravité", PhD Thesis, Université d'Orléans, Orléans, France, 2014.

[29] J. G. Wilson, *The principles of cloud-chamber technique*, Cambridge Monographs on Physics, Cambridge University Press, 2014.

[30] D. Kaya, G. Renoux, F. Halter, A. Yozgatlıgil, I. Gökalp, C. Chauveau, "Evaporation of a single ethanol droplet interacting with a premixed laminar CH_4/air flame", in *ICLASS 2021, 15th Triennial International Conference on Liquid Atomization and Spray Systems*, 2021.

[31] F. Thiesset, F. Halter, C. Bariki, C. Lapeyre, C. Chauveau, I. Gökalp, L. Selle, T. Poinsot, "Isolating strain and curvature effects in premixed flame/vortex interactions", *J. Fluid Mech.* **831** (2017), p. 618-654.